10th ESA Workshop on
Advanced Space Technologies for
Robotics and Automation

EXPERIENCES GAINED FROM THE THERMAL VACUUM TESTS OF THE MICROROVER NANOKHOD

Authors: Sabine Klinkner[1,2], Chris Lee[1], Carsten Wagner[1], Michael Lengowski[2], Hans-Peter Röser[2], Pascale Bourlier[3]

Astra 2008

11. – 13. November 2008, at ESTEC
Nordwijk, the Netherlands

[1] ***von Hoerner & Sulger GmbH,***
Schlossplatz 8, 68723 Schwetzingen, Germany,
Email: klinkner@vh-s.de

[2] ***Universität Stuttgart, Institut für Raumfahrtsysteme,***
Stuttgart, Germany

[3] ***Harmonic Drive AG,***
Limburg, Germany

Abstract

With the recent development of the microrover Nanokhod for the demanding surface environment of the Mercury night side, the rover made a huge advance towards a practical flight model. The rover was designed by the company von Hoerner & Sulger GmbH under an ESA contract to meet the flight-model requirements for a Mercury surface mission. This means it has to withstand such extreme environmental settings as temperatures down to -180°C in vacuum conditions, a landing shock of 200 g for a duration of 20 ms and a surface material consisting of very fine regolith with an extremely low thermal conductivity. The hardware model based on these requirements was manufactured to an engineering level and is suitable for environmental testing of vibration, shock and thermal vacuum.

The first thermal vacuum tests of the rover system were successfully conducted and the results provide a good understanding of the thermal behaviours within the system. In addition, these results are used for the validation of the detailed thermal model of the rover which has been developed in parallel to the Nanokhod model. This validated model thus presents a powerful tool which can be used as a baseline for the future design steps of the thermal concept. It provides detailed information on possible hot spots in vacuum condition and helps to avoid them. A good understanding on the temperature distribution within the rover also helps to reduce the risks and uncertainties for the scientific instruments and critical electronic components.

In addition to the first environmental tests, the drive units of the rover system were also subject of further analysis. For the new rover development the drive unit had to be redesigned to match the environmental requirements of the Mercury surface. Unfortunately the framework of the project did not allow for a workbench setup of the drive system before the integration into the small scale rover volume. This lead to some initial blocking problems. These problems could be solved by a run-in and some adjustments of the drive; the rover now works fine. Nevertheless, for the benefit of a future flight model the drives have been thoroughly tested to have a good understanding of the different factors having an influence on the drive unit and then to be able to provide a reliable drive system.

Although currently the mission to Mercury is very unlikely, the new design prepares the rover well for a number of alternative mission scenarios. Especially the detailed analysis of the thermal aspects of such a small and integrated system offers a perfect baseline for mass critical and thermally challenging requirements as for example on a mission to the moon poles.

This paper describes the results of the thermal vacuum tests of the rover as well as the lessons learned on the detailed drive analysis.

1 INTRODUCTION

The development history of the microrover Nanokhod under the leading role of *von Hoerner & Sulger GmbH* started in the early 1990's. Since then the original Russian concept has been adapted for several target surfaces like the Moon, Mars and Mercury. In the development for example, a package of three scientific instruments was accommodated into the rover. The current rover payload consists of two spectrometers - an Alpha-Particle X-ray Spectrometer and a Moessbauer-Spectrometer - and a Micro-imager. The development also included the building of microrover prototypes which were used to test the rover abilities, for example the driving performance on soil simulants.

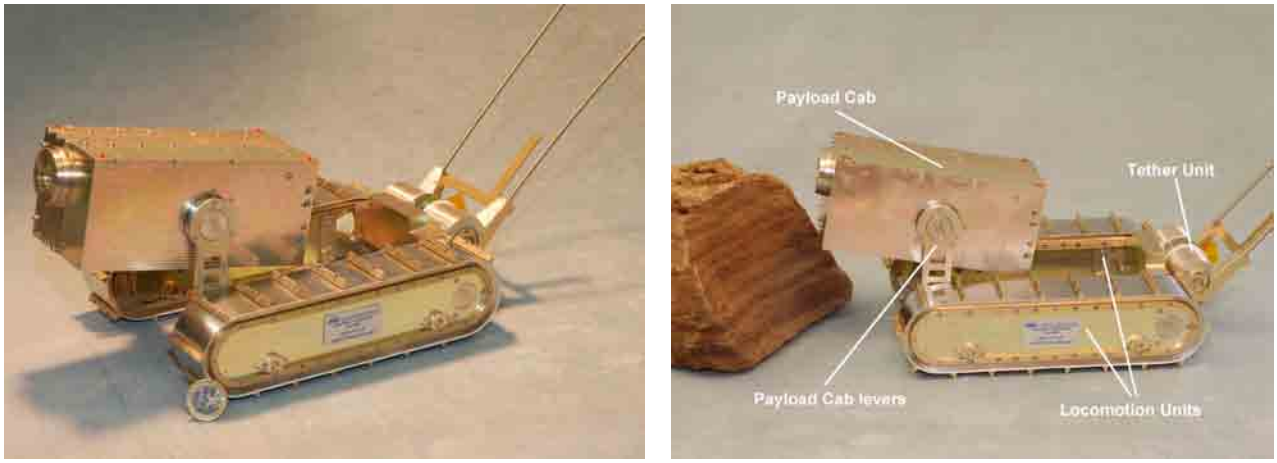

(a) For size comparison of the microrover

(b) Naming convention of the Nanokhod

Figure 1: MRP mircrorover Nanokhod

The Nanokhod rover is a small mobile scientific platform, designed to transport and operate scientific instruments for in-situ measurements of rocks and small craters in the vicinity of the landing point. The microrover has a volume of $160 \times 65 \times 250\,\mathrm{mm}^3$, it weighs 3,2 kg including a payload mass of 1 kg and it has a peak power of 5 W. The Nanokhod is a tethered system that uses the Lander for power supply and as its data relay to Earth. An impression of the rover size and the labelling of the main rover components are given in Figure 1.

In the course of the latest development the rover gained a near flight readiness with a practical design to withstand the tough requirements of a flight model for the Mercury surface [1]. Having realised a design that meets the flight-model requirements, a hardware model has been manufactured to an engineering level which is suitable for environmental testing of vibration, shock and thermal vacuum. This design is able to withstand such extreme requirements as temperatures down to $-180^{\circ}\mathrm{C}$ in vacuum conditions, a landing shock of 200 g for a duration of 20 ms and a surface material consisting of very fine regolith with an extremely low thermal conductivity.

Due to limited resources and delays within the original TRP study, the environmental tests of the model were discarded from the project. To still validate the rover model, further analysis and tests were conducted in the framework of an University project together with the IRS (Institute of space systems, Universität Stuttgart). These analyses included the development of a detailed thermal model of the rover and the first thermal vacuum test with a moderated thermal range. The results from the thermal model were used to optimise and validate the thermal model.

Further tests considered the drive unit of the rover. During the initial functional tests of the manufactured model, the drive unit caused some problems. Although the problem could extensively solved during the project, some further drive tests were carried out after the completion of the MRP project, to fully understand the problem. These tests analysed the effects of the drive unit in more detail and thus help to provide a reliable drive unit for any future implementation of the microrover.

2 THERMAL MODEL AND THERMAL VACUUM TESTING

For a complex system like the rover, a simple thermal estimation will give some first numbers and ideas in which dimension the temperatures will range for the required environmental conditions. However, in order to get representative limit values for the electronic parts or the scientific instruments, it is essential to model the rover system and the occurring environment in more details.

In parallel to the development phase of the rover the thermal model was build and refined to more and more detail. The first model was a simple spread sheet calculation giving temperatures in rough approximation. The second model is

designed with the help of a Design Compiler 43 and the ESATAN-/ ESARAD-Software. Based on the second model there has been a number of iterations on the thermal network considering areas of special interest and refining the network due to unexpected temperature measurements or on thermally sensible parts.

The rover breadboard was designed and built for testing purposes in a thermal vacuum chamber for the boundary conditions of the Mercury surface. This is why the thermal rover model was reconfigured to provide the boundary conditions of thermal chamber. The thermal model could thus be used to predict the temperatures for different conditions in preparation of the thermal vacuum tests. Additionally the modification of the model allowed using the test results to evaluate the model. Deviations between the temperature results of the test and the model are caused by the assumptions made on material properties and simplifications in the model, which can be improved or even completely resolved.

A thermal model calculation before the first thermal vacuum test, assuming the vacuum test boundary conditions of the thermal vacuum chamber, was conducted to show that the planned functional rover tests can be safely accomplished also for room temperature conditions. The model showed that the temperatures of the heat dissipating electronics would not exceed critical levels and damage could occur.

2.1 Objectives of thermal vacuum tests

The main objective of the thermal vacuum test is to verify the compatibility of the MRP design to the thermal vacuum environment. Although the facility used for the thermal vacuum testing was not able to reach the required temperature of $-180°C$, it allowed to test the system on relieved temperature levels, as a first qualification step of the rover system. Furthermore, the test provided data for the comparison with the calculations of the thermal model realised with ESARAD/-TAN.

There are two separate thermal vacuum tests in order to gain as much information as possible from the rover. The two tests allow a higher number of test data, as well as the possibility to have a closer look at specific temperature distributions during the second test after the evaluation of the first test data. Part of both thermal vacuum tests was a rover functional test for the verification of the rover system. The functional test involved the operation of the electronic system and the PLC mechanisms with the rover static on its tracks.

2.2 Comparison of test results and iterated thermal modelling results

The calculated temperatures of the thermal model were compared with data of each test. The comparison helped to optimise the thermal model by modifying some simplifications and assumptions, in order to achieve matching temperature curves. The results from the optimised model compared to the test data of the second thermal test show finally a good compliance. Still the temperature curves from the calculated and the measured data do not cover each other completely, due to simplifications within the model and effects of the temperature measurement. For example, one simplification effect in the model is, that the calculated temperatures are always an average value for the whole component. The effect is larger for components, which partially dissipate heat like the PCBs, due to the higher thermal gradient within the component. Also large components show a higher inaccuracy as the average temperature is taken over a larger volume.

Measurement divergences result from the fact that the temperatures are only determined on one surface of the component and thus depending from the conductivity within the component, the measured value will give only local information. Additionally the mounting of the thermistors on the surfaces has to consider the impact of thermal radiation effects from the surrounding components. The effect of the thermal radiation on the thermistor is quite high due to its low heat capacity in comparison to the component on which it is mounted.

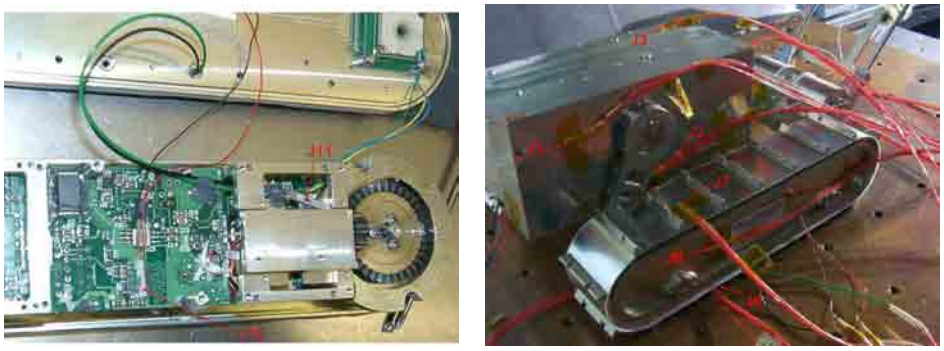

(a) Thermistors in the left locomotion unit (b) Thermistors on the left locomotion unit

Figure 2: Positioning of the thermistors on and inside the rover during thermal vacuum test

Figure 3 and 4 show the comparison of measured and calculated data on two heat dissipating and two purely passive component examples (figure 2).

The two heat dissipating components are inside the left locomotion unit (LU): The motor controller and the Payload Cabin (PLC) articulation motor located in the front of the left LU. The thermistors are indicated with J11 (motor) and J12 (controller PCB) in figure 2(a). The controller PCB is inside the track unit in-between the two side walls, to which it is mounted via aluminium standoffs. The electronics on the motor controller PCB are activated approximately half way through the functional test when the articulation motor in the locomotion unit is switched on.

The thermistors on the two passive components are sensor J7 and J8 on the track foil on the upper and lower side of the left locomotion unit, see figure 2(b).

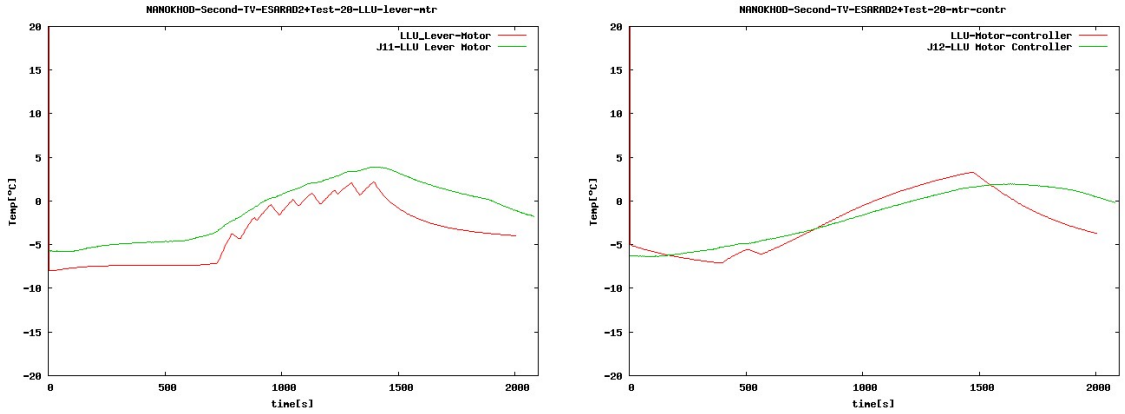

(a) LLU motor

(b) LLU motor controller

Figure 3: Comparison of the validated model results and temperatures of the second thermal vacuum test for the LLU motor components

Figure 3(b) shows a good compliance of the calculated and measured temperature of the motor controller. The calculated temperature shows a very distinctive curve, while the measured curve is following the same trend with a smoother line. The sensor is measuring a smoother temperature behaviour, as it is on the surface of the motor controller PCB, and thus the dissipated heat which is reaching the sensor is slightly damped. For the calculation the heat is dissipated directly within the component and thus the temperature curve follows the activation of the motor controller without delay.

The sensor directly on the articulation motor in the LU (figure 3(a)) shows that the calculated temperature matches nicely the measured temperature curve; however, the measured data is again less distinctive due to the position of the sensor. The sensor is mounted on the outside of the motor cradle where the maximum thermal resistance of the part applies. Opposed to the thermal resistance assumed in the calculation which is an average of the thermal resistance in the centre of the motor to the maximum thermal resistance on the surface of the cradle. At the same time the thermal radiation effects of the cold LU parts, which are surrounding the motor, affect the measurement of the thermistor. Thermal radiation from the motor controller also explains the slightly rising temperature value, before the articulation drive is activated.

Graph 4(a) in Figure 4 shows that the curves for the lower side of the track foil match quite nicely. The only differences are some waves in the measured curve during the activation of the articulation drive. These result from the rotation of the drive, providing a changed radiation interface to the sensor by moving a colder surface of the drive towards and then away from the sensor. The movement of the surface is not included in the thermal model and thus can not be seen in the calculated curve.

For the upper side of the track foil, the calculated and measured curve match very good (figure 4(b)), however the measured curve is always higher than the calculated one. This is caused by the assumption within the thermal model that the boundary nodes, a cooling plate below the rover and a shroud covering the rover, have each one temperature across their complete surface. However, the boundary nodes in the test have a gradient; the shielded area underneath the rover is much colder than the area surrounding the rover. Thus the model assumes a too low temperature for the area around the rover, when using an average temperature and on the opposite a too high temperature for the shielded area underneath the rover. Due to that the calculated temperature for upper side of the track foil is lower than the measured one.

Despite the slight deviations from the calculated and the measured temperature the model shows a good compliance with the real conditions in the test. All observed variations are marginal and can easily be explained by either the thermistor position or a simplification within the model.

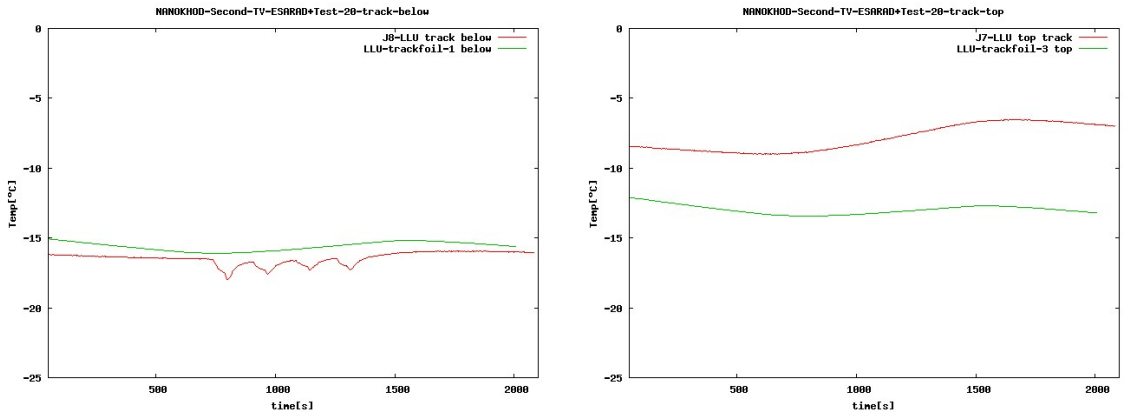

(a) LLU track below

(b) LLU above track

Figure 4: Comparison of the validated model results and temperatures of the second thermal vacuum test for the LU track foils

2.3 Influence on the thermal system design

The iterated model can now provide the temperature distribution of all rover components which could not be measured due to the limited amount of thermistors or a limited accessibility. Additionally the model can be used to implement different boundary conditions, in order to analyse the thermal behaviour of the rover within any implemented environment. Like that the model can disclose critical areas for the applied environmental conditions and allows the optimisation of the thermal system concept in case it becomes necessary. With these results the thermal system of the rover can be validated for the target environment of any mission.

The last iteration of the model implements the boundary conditions of the Mercury mission scenario for the Bepi-Colombo lander. The contact surface is assigned with a surface temperature of $-180°$C and with a thermal conductivity for regolith of $\lambda = 0,01$ W/mK.

A calculation was conducted based on the deployment and operation procedure for the first 48 h as foreseen for the BepiColombo lander mission. The scenario consists of the following rover activities, including the mentioned rover modes:

- **Checkout sequence**, including the rover modes Localisation, Science APXS, Science MIMOS, Science MIRO-CAM
- **Complete Path**, including the rover modes Locomotion, PLC Move, Localisation, Locomotion, Localisation
- **Measurement Sequence**, including the rover modes Locomotion, PLC Move, Science MIROCAM, PLC Move, Science APXS, PLC Move, Science MIMOS, PLC Move
- **RoverOff**

Figure 5 shows the temperature distribution within the rover after a Complete-Path activity (figure 5(b)) as well as after a Measurement-Cycle activity (Figure 5(a)).

In both cases the temperature within the rover varies between $\approx -44°$C on the hottest component and $-180°$C on the Mercury surface node. During the scientific measurements the highest temperature can be observed on the central controller PCB in the PLC. Also the PLC motor is quite warm due to the repetitive PLC rotation for the positioning of the instruments. And as the last instrument of the measurement cycle the MIMOS instrument is still on a temperature level of $\approx -70°$C.

For the locomotion mainly two areas have an increased temperature: The locomotion driver PCBs in the rear of each locomotion unit and slightly less the central controller PCB in the PLC. As shown on these two examples the model provides the thermal distribution within the system for any rover mode. Like that it defines the thermal boundary conditions which have to be applied for each component and thus supports any future design.

3 DRIVE TESTING

Tests on the drives system have clearly demonstrated that it is capable of producing sufficient torque for the application. However, during the initial testing of the rover the drive occasionally stalled whilst running. Investigations indicated that

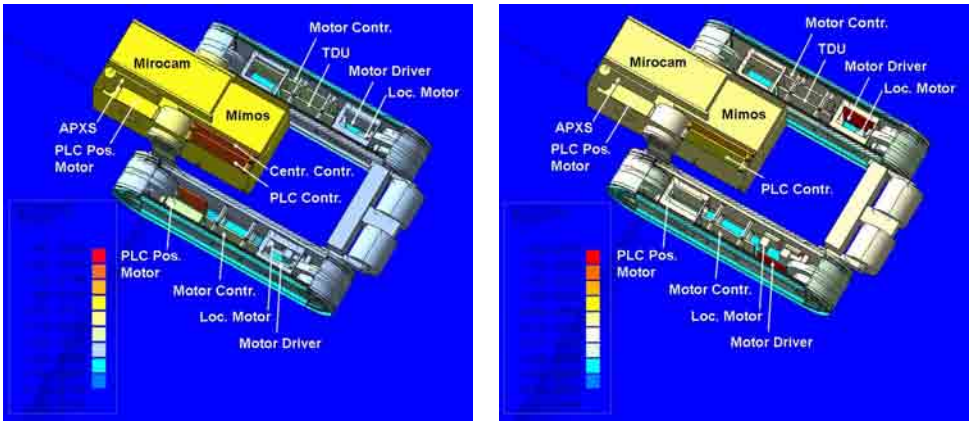

(a) Rover after science cycle

(b) rover after locomotion

Figure 5: Temperatures in the rover after science cycle and locomotion activity

a number of factors are causing the torque of the stepper motor to be reduced below the required limit. The variation in the drive torque can cause the motor to miss a step. The problem is that a stepper motor is unable to run immediately at the operational speed and requires a controlled acceleration ramp, which means if the motor misses a step due to a torque peak, it will stall. As the stepper motor is driven with an open loop control the motor does not recover autonomously from the this situation. Several examinations have been carried out, when the stalling of the drive occurred during the functional tests of the rover, with the following results:

- Software/electrical drive problems are discounted after tests.
- Stalling position suggests no single tooth of crown/pinion gear is responsible for the stopping of the motor.
- Load is a factor in the frequency of occurrence.
- The problem occurs more often in one direction of output shaft (but opposite for the two PLC drives). The crown gear is mounted in different orientation for the PLC- (teeth towards HD) and the Lever-drive (teeth away from HD). This means that the same crown gear face is causing the higher probability of errors. This can be an indication for a machining error.

Motor tests on a spare motor showed that the clamping of the motor body caused the motor to stop, but also that it is capable to produce more than the required torque. The re-testing of the drives while improving the method of clamping the motor showed some improvement. Another improvement could be achieved by enlarging the distance between pinion and the gear wheel of the crown gear to a higher value than required by the gear setup tolerances. The bigger distance reduced the radial loads on the planetary gear axis which have caused a reduction of torque.

Still the problem could not be completely solved and the stalling kept occurring occasionally. However the problem appeared less frequently the longer the drives were running. Some running-in effect seemed to improve the situation. This fact correlates very well with the friction characteristics of Dicronite lubricant over the number of revolutions [2]: The friction is approximately 3 to 4 times higher for the first revolutions, after a running-in time it is dropping to the low friction coefficient of 0,03, before it is suddenly rising excessively at the end of its lifetime.

The mounting tolerances over the whole drive system interfaces are another probable factors leading to the reduction of torque margin. The Harmonic Drive unit comprises already nine interfaces. Also the dry lubricant may increase the stiction forces of the faces of the gear teeth. All effects are exacerbated by the small scale of the components relative to the used torque levels. Although the problem seemed to disappear after the running-in of the system, the drive was carefully examined in two tests:

The tests were carried out at the Harmonic Drive AG laboratory and were considering the validation of the drive system and its margin. The objective of the first test was to inspect the MRP drive unit (consisting of the planetary gearhead, the crown gear and the Harmonic Drive unit (HFUC-5-100) driven by the stepper motor AM1020), when mounted in a stiff environment on the test bench. The test setup provided assessments of torque variations on the output as well as acceleration measurements. The objective of the second test was to verify the torque loads specifically in the Harmonic Drive stage during the revolutions of the gear. The second drive setup was done with a DC motor in order to monitor the current which directly relates to the required torques.

3.1 MRP drive unit test with stepper motor

For the test a 50 cm arm is attached to Harmonic Drive flexspline output of the LU lever drive to apply torque to the drive. The arm has a bucket on the other end to add weight to adjust the torque on the drive. The arm starts from vertical downwards position and moves counter-clockwise to the horizontal position. With an unloaded bucket the maximum torque in the horizontal position is 0,35 Nm. By adding weight in steps of 60 g the torque applied to the drive is raised to max. 2,7 Nm. For each load step the arm is driven counter-clockwise from the vertical to the horizontal and back down again. The test is repeated with three different step rates: the nominal step rate of 1528 steps/s, the step rate of 934 steps/s and the slowest steprate of 104 steps/s. The test-setup is shown in figure 6.

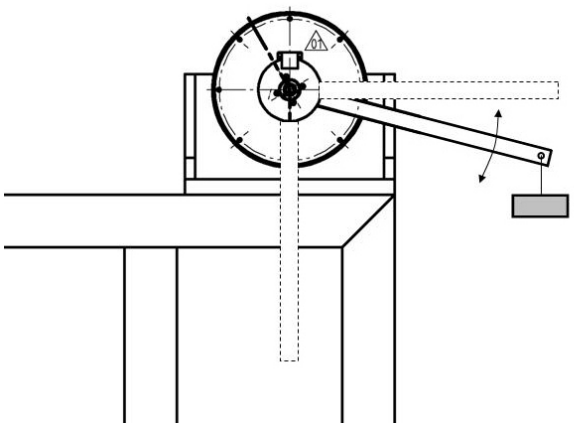

Figure 6: Test setup of drive tests

The inductance of the motor windings of a stepper motor changes when load is applied [3]. In-between two steps of the motor the application of the voltage moves from one coil to the next. The so called rise time that is needed for the current to build up in the new coil and is dependent from its inductance. With a higher load the inductance decreases and the rise time is shorter. Thus the measurement of the rise time indicates the torque load applied to the motor. For the detection of torque variations during the test, an oscilloscope measures the voltage and the current and gives a trend of the rise time over a period of 20 sec.

During the tests no stalling of the drive system occurred, nevertheless the measurements of the first test confirmed the suspicions for causes of stalling. The measurement results for the test with minimum and maximum torque load and for the nominal step rate are shown in the figure 7. The graphs present the rise time for the switching of the motor coils in-between two steps applied over the time to lift the arm from vertical to horizontal. The graphs show a clear trend – the green line –, derived from an average over 40 values, of decreasing rise time and thus increasing torque, for the loads applied. This trend becomes more obvious when applying a higher load. Spikes of shorter rise time in both graphs indicate several torque peaks during the lifting. This explains the higher occurrence of the problem with higher torque loads, as the torque peaks add to the general load and thus can lead to torque levels which are larger than the motor margin allows for.

An acceleration sensor was attached to the output of the drive. At first sight, its measurements reveal no influence of the different gear stages as the results are too noisy. In order to see if the data is a combination of sinusoidal basis functions which identify specific influences, a Fast Fourier Transformation (FFT) analysis is carried out on the data of the acceleration sensor. The comparison of the FFT analysis for the nominal step rate with medium and maximum load applied to the torque arm (figure 8), shows the noisiness of the acceleration data. However, for both torque loads the same two frequencies show the highest amplitude, in the range of ~ 22 Hz and in the range of ~ 47 Hz.

The amplitude of these frequencies varies with the torque load. Tests with slower steprates revealed, that the system shows the same peaks, even though the stimulated frequencies of the different gear stages are lower for the slower speeds. The amplitude of the frequencies is the only parameter that varies with the motor speed and the torque load. The fact that the frequency is the same for all motor speeds implies that this is the Eigen-frequency of the gear unit setup. A comparison with the frequencies of the different gear stages in table 1 does not indicate that the Eigen-frequency is driven by an irregularity of one of the gear stages.

However the impact of the gear-stages can not be completely disregarded as it might be covered by other effects. Unfortunately the MRP project did not allow for careful testing of the separate gear stages before assembling the unit and integrate it into the rover. A following phase should include a comprehensive test campaign, which is analysing the single drive stages as well as the unit. Only the proper analysis of the drive unit will provide a reliable drive system the rover can rely on.

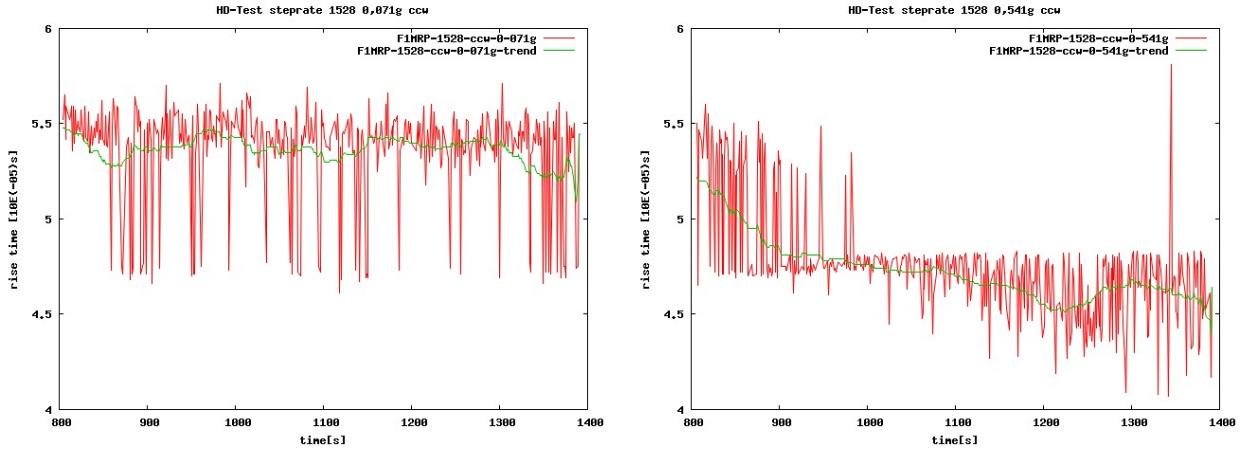

(a) Torque load $0,35$ Nm (b) Torque load $2,70$ Nm

Figure 7: Rise time distribution over a 90° counter-clockwise output movement for minimum and maximum load and the nominal step rate of 1528 steps/s

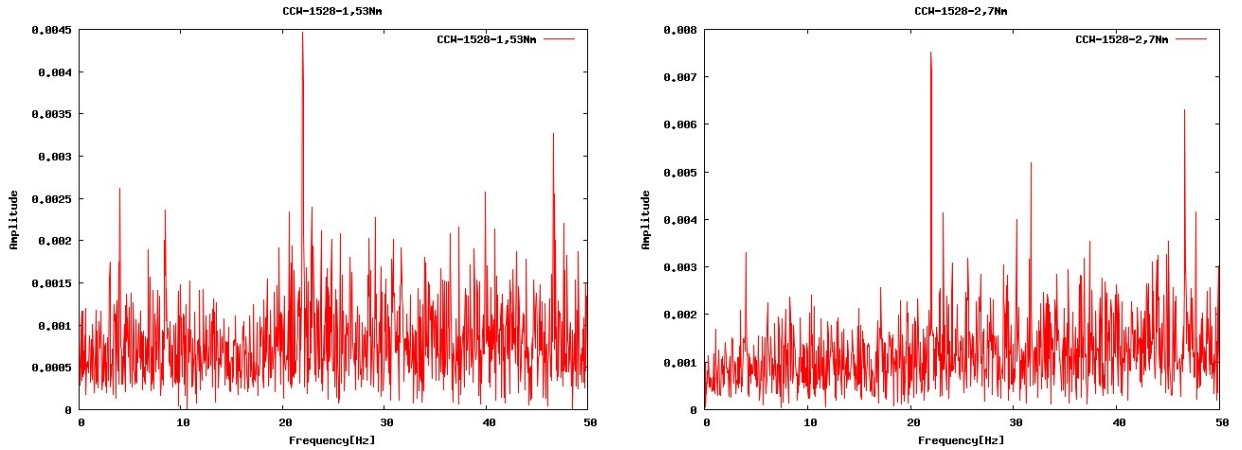

(a) Torque load $1,53$ Nm (b) Torque load $2,70$ Nm

Figure 8: FFT- analysis for stepper-drive tests with different applied torques loads and the nominal step rate of 1528 $steps/sec$

	Step rate 1528 steps/s	
Gear stages	Angular frequency [rad/s]	Frequency [Hz]
Harmonic Drive	0,49	0,08
Crown gear	1,19	0,19
Planetary Gearhead	76,34	12,15

Table 1: Frequencies of the drive stages for the different motor speeds

3.2 MRP drive unit test with DC-motor

The objective of the second test is to verify the torque loads specifically in the Harmonic Drive gear stage. In this test the Drive unit is disassembled and only the Harmonic Drive stage is setup for the test and driven by a DC motor. The application of torque loads is done in the same way as for the stepper motor tests: The drive is mounted onto a rigid test bench. A load arm is applied to the output of the Harmonic Drive. The arm is driven counter-clockwise from the vertical to the horizontal position with different loads added on the other end of the arm, providing an increasing torque for the lifting of the arm. Measurement devices record the input torque needed to back-drive the gear. The test shall verify if the torque peaks which were observed in the stepper motor setup can be detected also in the Harmonic Drive stage. The input speed on the Harmonic Drive input side is 26 rpm.

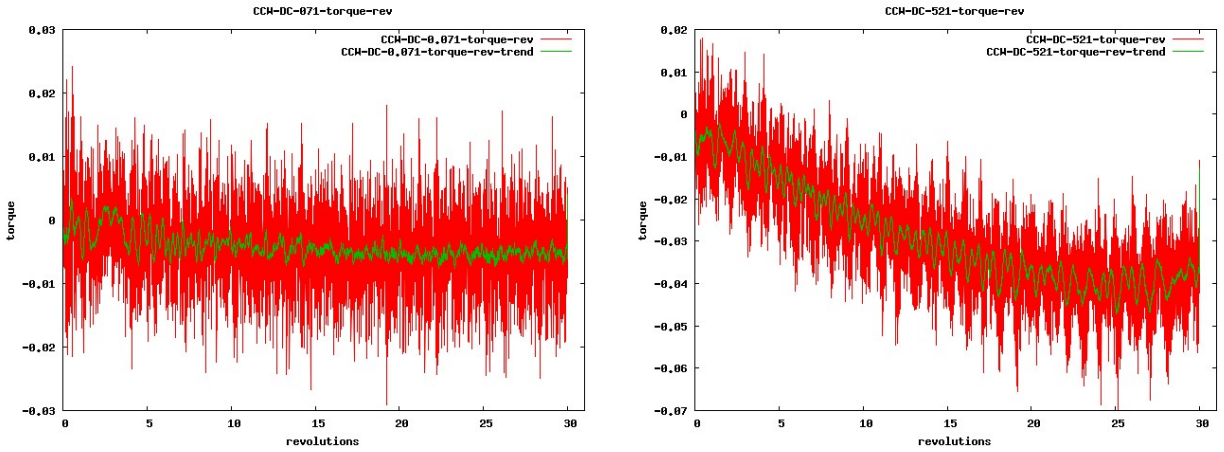

(a) Torque load DC0, 35 Nm

(b) Torque load DC2, 55 Nm

Figure 9: Back-drive torque over a 90° counter-clockwise output movement for different loads

The graphs in figure 9 show the back-drive torque for two different load cases. As expected, the trend (derived from an average over 40 values) shown as a green line of the back-drive torque is deflected from the zero axis for an increasing load of the arm travelling from vertical to the horizontal position. This effect becomes more obvious for an increasing torque load. Torque peaks as for the stepper motor tests can not be detected. However, the measured data is relatively noisy resulting from the sensitive drive control. This means possible peaks could be covered by the noise. The separate test of the Harmonic Drive unit does not indicate any irregular running of the Harmonic Drive.

The Eigen-frequencies derived from the FFT of the acceleration data and shown in figure 10 do not correspond with the frequencies of the drive unit rotation, given in table 2. Due to the disintegration of the drive unit, the Eigen-frequencies for the DC test differ from the Eigen-frequencies of the stepper motor setup. The impact of the different applied torque loads becomes again obvious in the variation of the frequency amplitudes.

Gear stages	DC	
	Angular frequency [rad/s]	Frequency [Hz]
PMA	0,43	0,07
Harmonic Drive	43,35	6,90

Table 2: Frequencies of the Harmonic Drive for the DC motor test

3.3 Thermal test of an alternative actuator - the brushless EC10

In the course of the project an alternative actuator came on the market. The brushless EC10 is of a similar size than the currently applied motor AM1020 and it is able to provide a higher torque as well as a higher output speed of the rover. In the framework of the drive system analysis a cold test of this motor was conducted. This test was conducted to verify the function of the brushless motor for the temperature range down to $-180°$C.

The first test with a sensorless motor showed that the motor works down to $-180°$C. Further tests with a brushless EC10 including a hall-sensor showed that the motor still works reliably to the low temperatures, however the hall sensor signal fails. The signals started disappearing at a temperature of $\sim -80°$C.

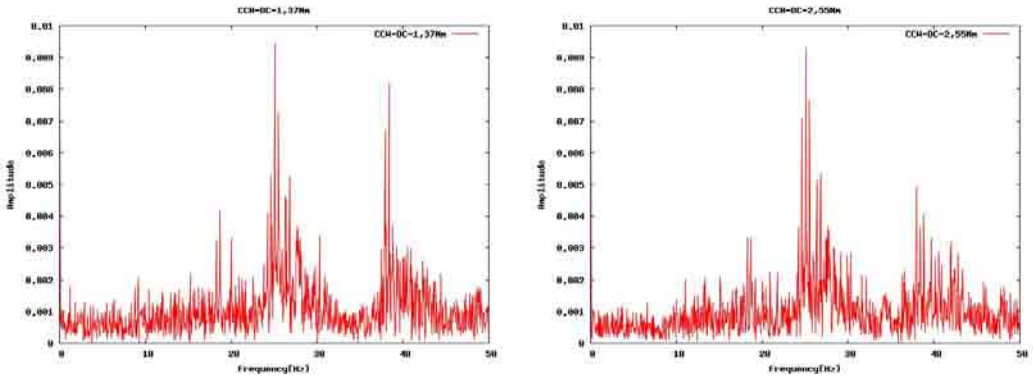

(a) Torque load $1,37 Nm$ (b) Torque load $2,55 Nm$

Figure 10: FFT analysis of the acceleration data for PMA–drive tests with different applied torque loads

For the purpose of using the brushless DC motor for the rover drive design the encoder unit of the motor has to be reviewed. In order to have the brushless DC motor as a promising alternative actuator the hall sensor could be replaced with another encoder type, which works reliably down to $-180°$C.

The implementation of the brushless DC-motor with a customised encoder, allows for a bigger torque margin, resulting into a more reliable drive unit.

4 CONCLUSION

The development of the miniaturised robotic space system Nanokhod made a big step forward in direction of the flight model. On the mechanical side the Nanokhod rover was developed from a concept stage to an engineering model, which is able to withstand the demanding conditions of a Mercury mission. Additionally the new rover design was optimised concerning the critical resources of volume, mass and power. The current design represents a highly integrated, mobile payload which can be flexibly implemented on a variety of missions for the exploration of planetary surfaces.

The extreme environment made it necessary to develop a more sophisticated thermal rover model. The development of the model was optimised and validated in the first two thermal vacuum tests of the rover systems. The validated model can now be used to predict temperatures of specific components. This makes the choice of components less risky and thus less cost intensive when carrying out the next design steps. The thermal model additionally allows an easy reassessment of the thermal design, e.g. for alternative mission scenarios.

On the mechanical side the solution of a reliable drive implementation was analysed to far extends. However the next design step shall foresee further work on that issue: The development of a suitable encoder for the brushless DC motor solution should be included. It is essential to qualify the drive components separately from the rover on an equivalent test bench which allows detailed measurement of the performances. This ensures that all contributing factors can be fully identified before implementing them in the complete drive unit. The test described in this paper provide already valuable experiences and thus provide a good baseline for further tests and for a reliable drive unit solution.

The rover is at a high state of development; although no mission opportunities currently exist, it is expected to be seriously considered for future missions to the Moon, Mars and other destinations.

References

[1] Klinkner, S., et al, *Destination Moon and beyond for the Microrover Nanokhod*, DGLR International Symposium, Bremen, Germany, Mar. 2007

[2] Anderson, M.J., Cropper, M., Roberts, E.W., *The Tribological Characteristics of Dicronite*, ESTL,ESR Technology Ltd. UK, 2007

[3] Schlienz, U., *Der Schrittmotor der nicht ausrastet*, WEKA FACHMEDIEN GmbH, 2007

[4] Barbé, J., *Mercury Thermal Model*, ESTEC-Noordwijk, (Aug. 2003)